AIP | Review of Scientific Instruments

Genetic algorithms applied to reconstructing coded imaging of neutrons and analysis of residual watermark

Tiankui Zhang, Huasi Hu, Qinggang Jia, Fengna Zhang, Da Chen, Zhenghong Li, Yuelei Wu, Zhihua Liu, Guang Hu, and Wei Guo

Citation: Review of Scientific Instruments **83**, 113505 (2012); doi: 10.1063/1.4765701
View online: http://dx.doi.org/10.1063/1.4765701
View Table of Contents: http://scitation.aip.org/content/aip/journal/rsi/83/11?ver=pdfcov
Published by the AIP Publishing

Genetic algorithms applied to reconstructing coded imaging of neutrons and analysis of residual watermark

Tiankui Zhang,[1] Huasi Hu,[1,a)] Qinggang Jia,[1] Fengna Zhang,[1] Da Chen,[1,2] Zhenghong Li,[3] Yuelei Wu,[1,4] Zhihua Liu,[1] Guang Hu,[1] and Wei Guo[1]
[1]*School of Energy and Power Engineering, Xi'an Jiaotong University, Xi'an 710049, China*
[2]*College of Material Science and Technology, Nanjing University of Aeronautics and Astronautics, Nanjing 210016, China*
[3]*Institute of Nuclear Physics and Chemistry, CAEP, Mianyang, 621900 Sichuan, China*
[4]*Nuclear and Radiation Safety Centre, State Environmental Protection Administration (SEPA), Beijing 100082, China*

(Received 25 July 2012; accepted 19 October 2012; published online 27 November 2012)

Monte-Carlo simulation of neutron coded imaging based on encoding aperture for Z-pinch of large field-of-view with 5 mm radius has been investigated, and then the coded image has been obtained. Reconstruction method of source image based on genetic algorithms (GA) has been established. "Residual watermark," which emerges unavoidably in reconstructed image, while the peak normalization is employed in GA fitness calculation because of its statistical fluctuation amplification, has been discovered and studied. Residual watermark is primarily related to the shape and other parameters of the encoding aperture cross section. The properties and essential causes of the residual watermark were analyzed, while the identification on equivalent radius of aperture was provided. By using the equivalent radius, the reconstruction can also be accomplished without knowing the point spread function (PSF) of actual aperture. The reconstruction result is close to that by using PSF of the actual aperture. © *2012 American Institute of Physics*. [http://dx.doi.org/10.1063/1.4765701]

I. INTRODUCTION

In order to explore a new energy source and to resolve the anticipated energy crisis, some countries which lead in nuclear technology, such as the United States, France, and other countries, have been doing research of inertial confinement fusion for long time.[1–9] Up to now, fusion capsule driven by Z-pinch has been well developed. In diagnosis of the process, the designed field-of-view (FOV) should be larger than plasma region for tolerating misalignment.[10] A large FOV encoding aperture has been developed to diagnose the capsule driven by Z-pinch. The encoding aperture is derived from thick aperture.[11,12]

The GA is currently recognized as the best globally well-adapted optimization algorithm,[13–15] which has been successfully employed in penumbral imaging reconstruction by Chen.[16,17] However, its efficiency is low. Thus, being combined with convolution realized by fast Fourier transform (FFT),[18] GA could simultaneously assure the effectiveness and efficiency of the search. The required coded image in terms of neutron energy deposition in scintillating fiber array could be also simulated by MCNP code.[19]

A new phenomenon is discovered in our study. Residual watermark unavoidably appears in reconstructed images, while the peak normalization is employed in GA fitness calculation. Residual watermark is primarily relative to the shape and other parameters of the encoding aperture cross section. The properties and preliminary causes of the residual watermark are analyzed. In addition, the identification on equivalent radius[3,20] of aperture is established. By using the equivalent radius, the reconstruction can also be accomplished without knowing the point spread function (PSF) of actual aperture. The reconstruction result is close to that by using PSF of the actual aperture.

II. THE SIMULATION OF THE NEUTRON CODED IMAGING

The simulation model of neutron coded imaging using MCNP is shown in Figure 1. The deuterium-tritium fusion neutron spectrum was employed, and the peak energy is 14.08 MeV. The designed system magnification factor is 5, and the encoding aperture according to Ress,[11,12] with 6 cm length, is made of tungsten. The scintillation fiber array consists of 199 × 199 BCF-10 fibers of 500 μm diameter and 10 cm length. The system is set in air, and the neutron scattering in the air is neglected. The interaction between neutron and encoding aperture has been simulated with bias sampling technique. And the simulation also involves the process of neutron energy deposition in scintillation fiber array. The geometrical parameters in simulation is shown in Table I, the particle number is the number of the neutrons released from source surface in bias sampling angle, and the statistical fluctuation and the corresponding yield are also listed.

TABLE I. Parameters in simulation.

Particle number	Statistical fluctuation	Neutron yield in source area
108 535 000	0.0402	9.8×10^{10}

a)Author to whom correspondence should be addressed. Electronic mail: huasi_hu@mail.xjtu.edu.cn.

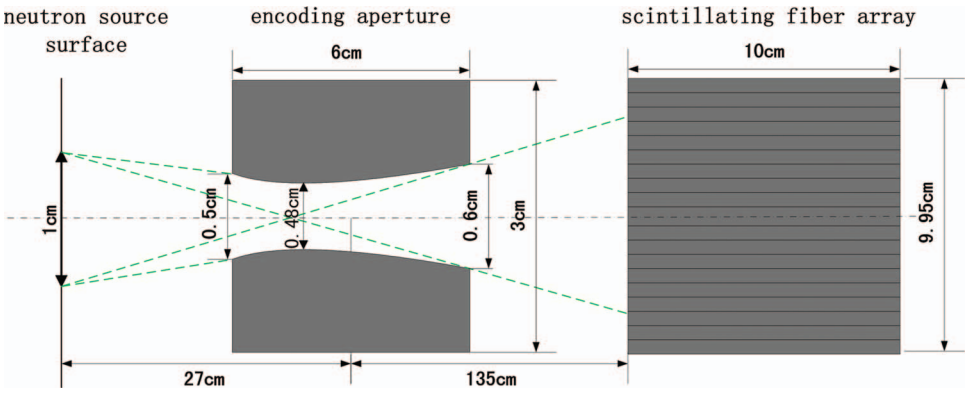

FIG. 1. Simulation model in MCNP.

The neutron source of pill region is set as "E" character, shown in Figure 2(a), and Figure 2(b) is its corresponding coded image.

III. GENETIC ALGORITHM AND RECONSTRUCTION

A. Flow chart of genetic algorithm

Figure 3 shows the flow chart of GA including the acquisition of neutron penumbral imaging and its point spread function by Monte Carlo method or experiment. In this study, the original image of pill is set up to be a binary image. If the neutrons are yielded from a pixel, this pixel value equals 1, and vice versa. The binary image model to be used for describing the image is conveniently to carry out operation by GA.

Following are major operators of GA: selection operator, crossover operator, and mutation operator. The selection process is usually combined with Elitist model[15,21] to guarantee the survival of the best individual. The crossover operator of binary image, playing roles as multiplication and inheritance of gene, employs uniform or random R/C (row/column) crossover[16] and window crossover[22] methods. The mutation operator is based on neighborhood pixel variation strategy and may be used to smooth images.[16]

B. Fitness value

According to Darwin's theory of evolution, some creatures owning stronger ability to adapt themselves to environmental change have better opportunity to survive and may have more descendants. The most important expression which describes the survival and reproduction of individuals is the fitness value or evaluation index.

In flow chart (Figure 3) of GA, the fitness value is defined as Euclidean distance, expressed in formula (3), to represent the deviation of an individual from source image of the pill. However, the individual image, obtained by binary image folded with PSF via FFT method, requires normalizing operation before doing fitness calculation. There are two main normalizing operations, one is peak normalization, and another is area normalization. In the operation of peak normalization, the operator $N(g(x, y))$ equals to the max value

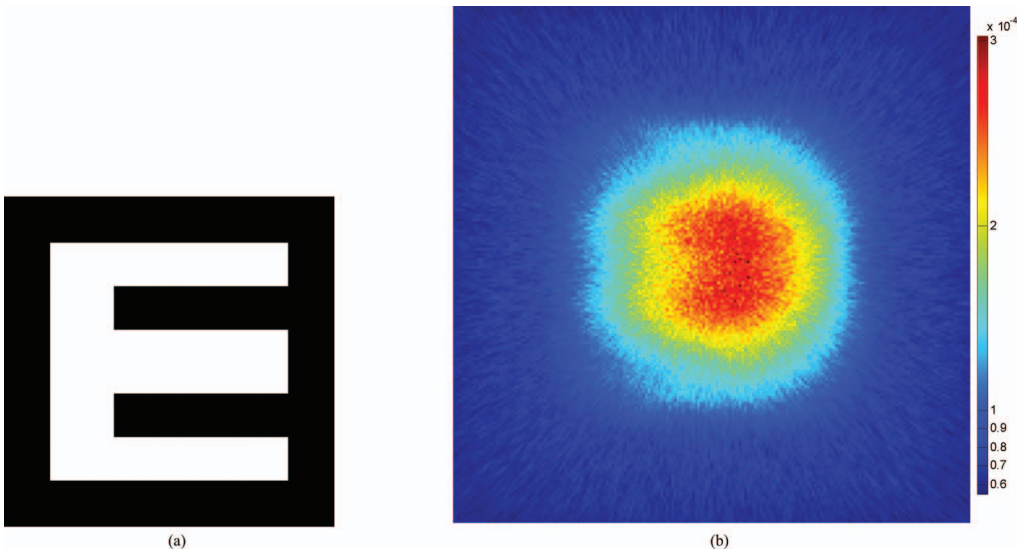

FIG. 2. The neutron source of "E" and its image: (a) the 7.15 mm size as pill region image, (b) simulation result.

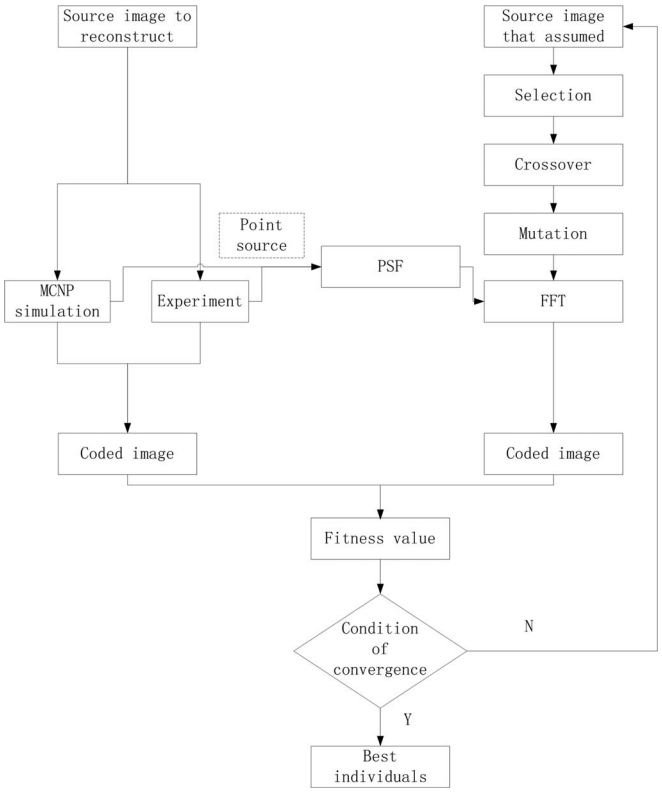

FIG. 3. The flow chart of GA.

of $g(x, y)$ expressed as $N(g(x, y)) = \max\{g(x, y)\}$. And, in the operation of area normalization the operator $N(g(x, y))$ equals to the summation of each pixel value expressed as $N(g(x, y)) = \sum\sum g(x, y)$,

$$\overline{g(x, y)} = \frac{g(x, y)}{N(g(x, y))}, \tag{1}$$

$$\overline{g_i(x, y)} = \frac{g_i(x, y)}{N(g_i(x, y))}, \tag{2}$$

$$f_i = f_C - \sum\sum \left[\overline{g_i(x, y)} - \overline{g(x, y)}\right]^2. \tag{3}$$

Where $g(x, y)$ and $g_i(x, y)$ represent the target image calculated by MCNP and the individual image produced by source binary image folded with PSF, respectively. f_C is a certain constant which guarantees that the fitness value of individual marked i, f_i , is positive.

TABLE II. Parameters of GA.

Parameters	Value
Population size	70
Generation maximum	3000
Size of Stochastic tournament	3
Probability of uniform R/C crossover (frequency)	0.2(1)
Probability of random R/C crossover (frequency)	0.2(1)
Probability of window R/C crossover (frequency)	0.0(0)
Probability of neighborhood mutation	0.001

C. Image reconstruction based on area normalization

There are three kinds of image reconstruction algorithms, individually by Richardson-Lucy (RL) method,[23–25] Wiener filtering,[26] and GA based on area normalization, shown in Figure 4. The input parameters of GA are listed in Table II. Unfortunately, both RL method and Wiener filtering require prior parameters, the number of iterations and signal-to-noise ratio (SNR). Here, correlation coefficient in expression (4) to evaluate the performance of reconstruction is introduced to determine the optimal prior parameters. The closer to 1 the value of correlation coefficient is, the more similar the reconstructed image is to the pill source image. To be highlighted, however, the truth is that the source image is unknown. But reconstructed image of RL method and Wiener filtering are depended on prior parameters which are difficult to determine. Hence, GA is more robust in experiment condition

$$r = \frac{\sum\sum f(i, j)\hat{f}(i, j)}{\left[\sum\sum f^2(i, j)\sum\sum \hat{f}^2(i, j)\right]^{\frac{1}{2}}}. \tag{4}$$

RL method owns the best reconstruction performance which has the best correlation coefficient, listed in Table III. The result from Wiener filtering seems blurry though it has a better correlation coefficient value than GA result. In view of image connectivity and distinction of edge, RL and GA show better adaptability for image reconstruction of fusion neutron yield image.

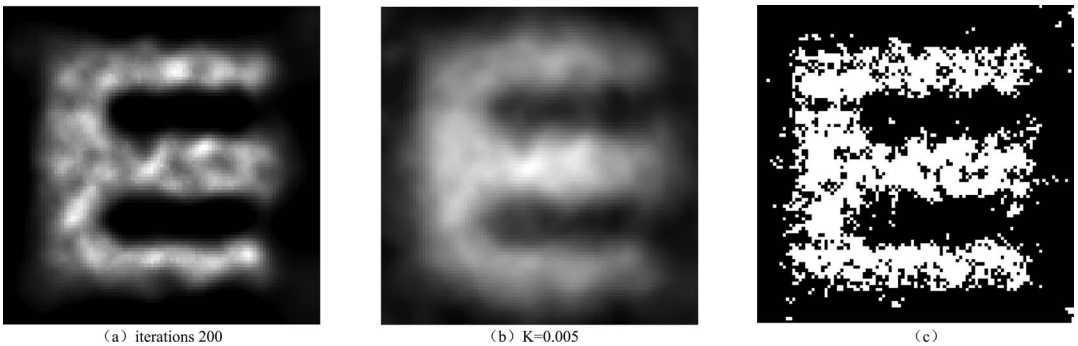

FIG. 4. Reconstruction source image by RL method (a), Wiener filter (b), and genetic algorithms (c).

TABLE III. Correlation coefficients of the results obtained by three reconstruction methods.

Reconstruction methods	Correlation coefficient
RL method	0.9309
Wiener filtering	0.8571
GA	0.7783

IV. RESIDUAL WATERMARK AND ITS CAUSE OF FORMATION

A. Residual watermark

Certain extra information (Figure 5), which overlies the reconstructed image in fitness calculation based on peak normalization, distinguishes obviously from the source image. This image information has not been reported in relative researches yet and is nominated as residual watermark.

Properties of residual watermark are studied and shown in Figures 6–10. In each figure, the sub-figure (a) is the source image, while the (b) and (c) show the reconstructed image by peak normalization and area normalization, respectively. Compared with peak normalization, area normalization owns a better reconstruction without residual watermark.

Figure 6 shows reconstruction results of the source set as characters "XJTU," with a size of 6.75 mm. Residual watermark also appears in its reconstructed image, if peak normalization is employed in fitness calculation, as shown in Figure 6(b).

The reconstruction results of the source areas in different sizes (2.2 mm and 6.6 mm) are shown in Figures 7 and 8. While peak normalization is employed, the residual watermark is unrecognizable in smaller source area (Figure 7(b)), in contrast it turns to be remarkable in bigger source area (Figure 8(b)).

The reconstruction results of images encoded by the apertures with different cross section shapes are shown in Figures 9 and 10. The aperture corresponding to Figures 9 and 10 is a square and a triangle cross section channel, respectively, and is derived from Figure 1. The source images used in simulations are the same shown in Figure 2(a). When the aperture with the square cross section channel is used, the square residual watermark can be observed in the reconstructed image with peak normalization (Figure 9); while the aperture with the triangle cross section channel is used, the triangle residual watermark can be observed in the reconstructed image with peak normalization (Figure 10).

FIG. 5. Residual watermark overlies reconstructed source image.

In order to study the relationship between the residual watermark and the GA, the GA program, GENOCOP4.0, developed by Michalewicz was applied and improved.[13,27] The main improvements were made on GENECOP4.0 in two aspects. On the one hand, FFT was applied to solve the fitness value. On the other hand, the suitable input file was prepared. In Figure 11 (source image is also the same shown in Figure 2(a)), the residual watermark does not appear in the reconstructed image with peak normalization. In another word, the appearance of residual watermark is largely dependent on search mode of GA. The correlation coefficient corresponding to Figures 11(a) and 11(b) is 0.6299 and 0.7103, respectively.

As mentioned above, the properties of residual watermark are represented as follows. First, the shape of residual watermark is independent of source image. Second, residual watermark is impacted by the size of source area. Third,

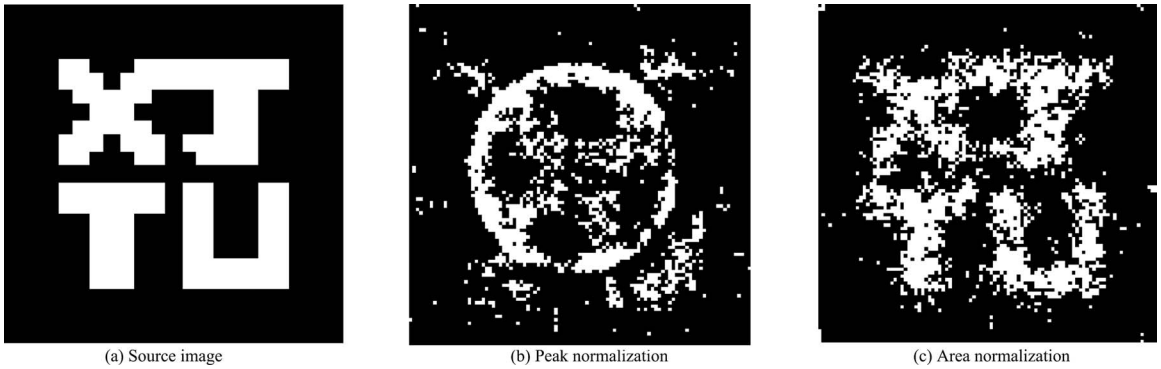

(a) Source image (b) Peak normalization (c) Area normalization

FIG. 6. "XJTU" characters with 6.75 mm size and reconstruction results based on two normalization methods: (a) source image, (b) peak normalization, and (c) area normalization.

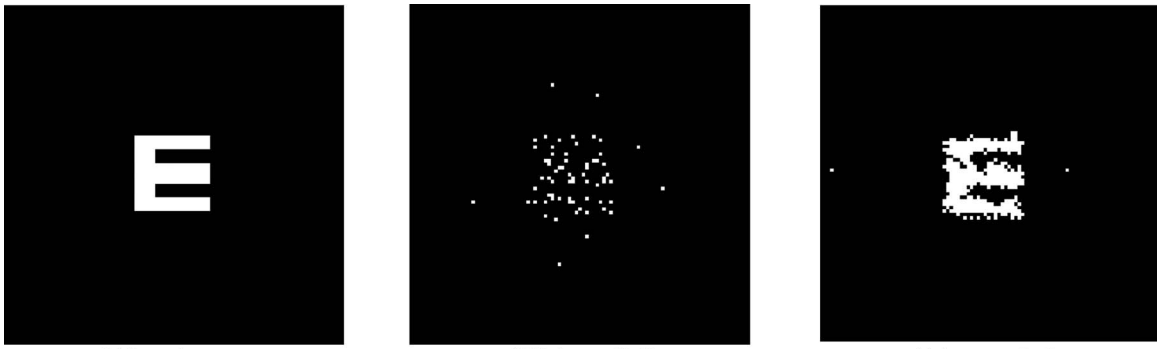

(a) Source image (b) Peak normalization (c) Area normalization

FIG. 7. "E" character with 2.2 mm size and reconstruction results based on two normalization methods: (a) source image, (b) peak normalization, and (c) area normalization.

residual watermark is related to the shape of the aperture channel cross section. Lastly, residual watermark is affected by search mode of GA. All in all, residual watermark is the relevant information of the cross section shape of the encoding aperture and appears once the size of source is roughly bigger than aperture radius.

B. The analysis of essential causes of residual watermark

In image pre-processing, image denoising for coded image was carried out by using adaptive Wiener filtering (AWF).[28] Then denoised image was applied to reconstruction based on peak normalization, as shown in Figure 12. The correlation coefficient corresponding to Figures 12(a)–12(c) is 0.7377, 0.7444, and 0.7071, respectively. With the operator scale of the selected filter (filtering denoising effects) increased, the information of residual watermark in peak normalization becomes unapparent. Therefore, the residual watermark comes from the weak signal which has high fluctuations and can be removed by denoising method. However, the reconstructed image of area normalization is less affected by this weak signal. On the contrary, the reconstruction performance of peak normalization is sensitive to weak signal.

In order to study the essential causes of residual watermark, as is shown in Figure 13, the information of image was carried by three kinds of neutrons: uncollided (trace "0"), large angle scattering (trace "1"), and small angle scattering (trace "2"), which interact with aperture material.

In order to study the contribution of these three kinds of neutrons to the reconstructed image, three specific encoding processes are taken into consideration. First, only uncollided neutrons involved, the coded result is shown in Figure 14(a), and the residual watermark overlies the reconstructed result in Figure 15(a). Second, provided large angle scattering neutrons are concerned, the coded image is shown in Figure 14(b), while both peak and area normalization methods give little information about source image or residual watermark in Figures 15(c) and 15(d). Lastly, if only small angle scattering neutrons are taken into consideration, the coded image is shown in Figure 14(c), and the reconstructed result is shown in Figure 15(e). Compared with the result in Figure 15(a), the reconstructed image in Figure 15(e) gives a distinct residual watermark.

The mean free path of neutrons in tungsten is of the order of 3 cm at 14 MeV.[29] The length of aperture is 6 cm, and aperture transmission in that case is about 13.5%. Indeed, the aperture transmission could give importance to aperture radiography similar to computed tomography scan and not to the source coded image itself.

The differences between area and peak normalization are important to understand the causes of residual watermark further and will be discussed in Sec. VI.

(a) Source image (b) Peak normalization (c) Area normalization

FIG. 8. "E" character with 6.6 mm size and reconstruction results based on two normalization methods: (a) source image, (b) peak normalization, and (c) area normalization.

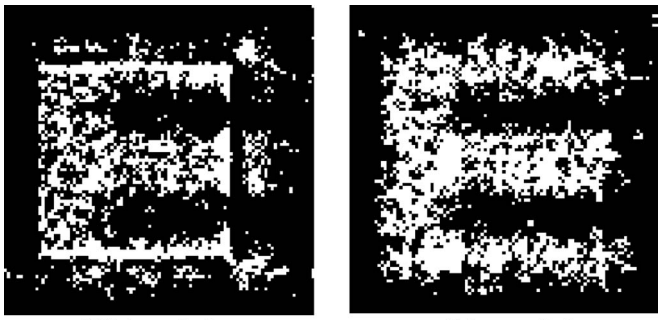

(a) Peak normalization (b) Area normalization

FIG. 9. Reconstruction results of "E" character coded by the aperture with the square cross section channel: (a) peak normalization and (b) area normalization.

(a) Peak normalization (b) Area normalization

FIG. 10. Reconstruction results of "E" character coded by the aperture with the triangle cross section channel: (a) peak normalization and (b) area normalization.

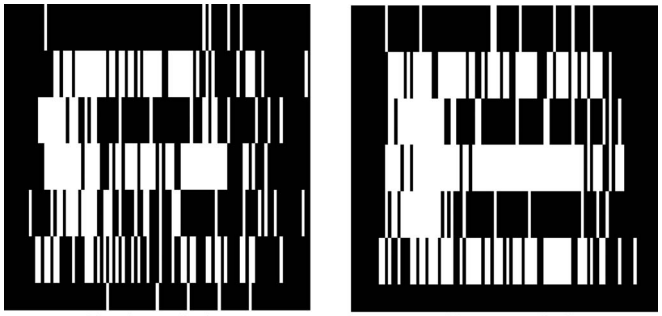

(a) Peak normalization (b) Area normalization

FIG. 11. Reconstruction results of "E" character reconstructed using improved GENOCOP4.0: (a) peak normalization and (b) area normalization.

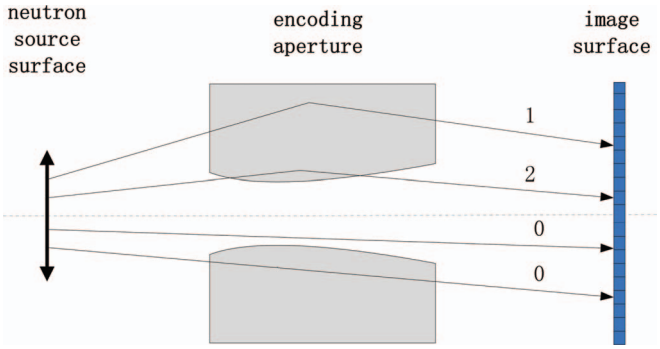

FIG. 13. The model of analyzing residual watermark.

V. APPLICATION OF RESIDUAL WATERMARK FOR IDENTIFICATION OF THE ENCODING APERTURE PARAMETERS

A. Information extraction from residual watermark

The Hough transform[30–32] was introduced as a method of detecting complex patterns of points in image data. It achieves this by determining specific values of parameters which characterize these patterns. The residual watermark overlies reconstructed image by peak normalization is a ring, shown in Figure 5, when the coding aperture is a round cross section channel. In this situation, the radius is the applicable parameter which characterizes the residual watermark. Radius of residual watermark was obtained by Hough transform. It is equal to 0.278 cm. Under the discussion of Sec. IV, the residual watermark changes in cross section of the encoding aperture channel, so it can be predicted that the radius of residual watermark should be related to that of the encoding aperture. To verify the relationship between theirs radiuses, single section of cylindrical encoding aperture was defined with the radius of residual watermark, PSF was obtained by simulating with MCNP code, and the image reconstruction was carried out by employing GA based on area normalization. The reconstructed image was shown in Figure 16. The correlation coefficient is 0.7153, which means the result is quite close to that reconstructed by using PSF of the actual aperture, listed in Table II. Therefore, the radius of the residual watermark is considered as the equivalent radius of the encoding aperture.[3,20]

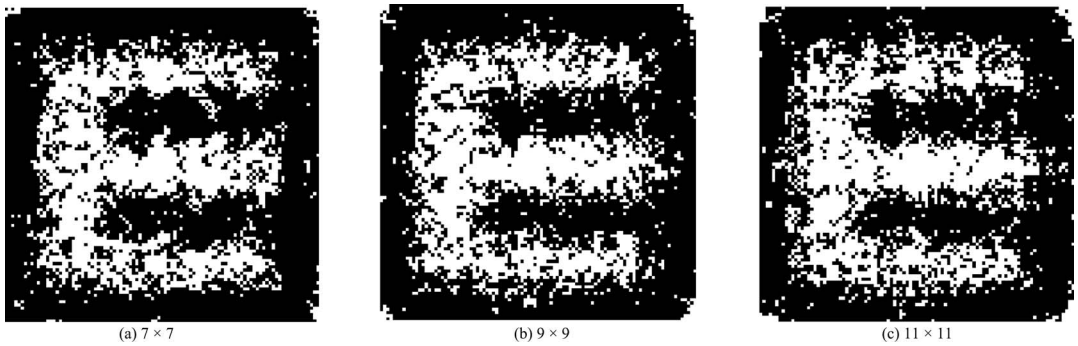

(a) 7 × 7 (b) 9 × 9 (c) 11 × 11

FIG. 12. The reconstruction results of the normalized peak after denoising by different AWF operator: (a) 7 × 7, (b) 9 × 9, and (c) 11 × 11.

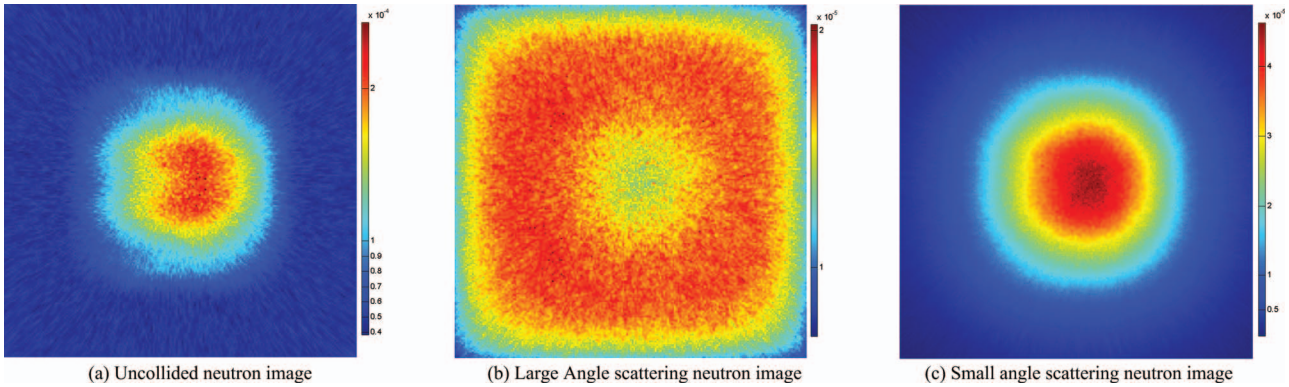

FIG. 14. The simulation result of "E" character source during different encoding process: (a) uncollided neutron image, (b) large angle scattering neutron image, and (c) small angle scattering neutron image.

B. Application of the residual watermark

The equivalent radius is obtained from residual watermark for actual aperture without knowing the PSF. The procedure is as follows.

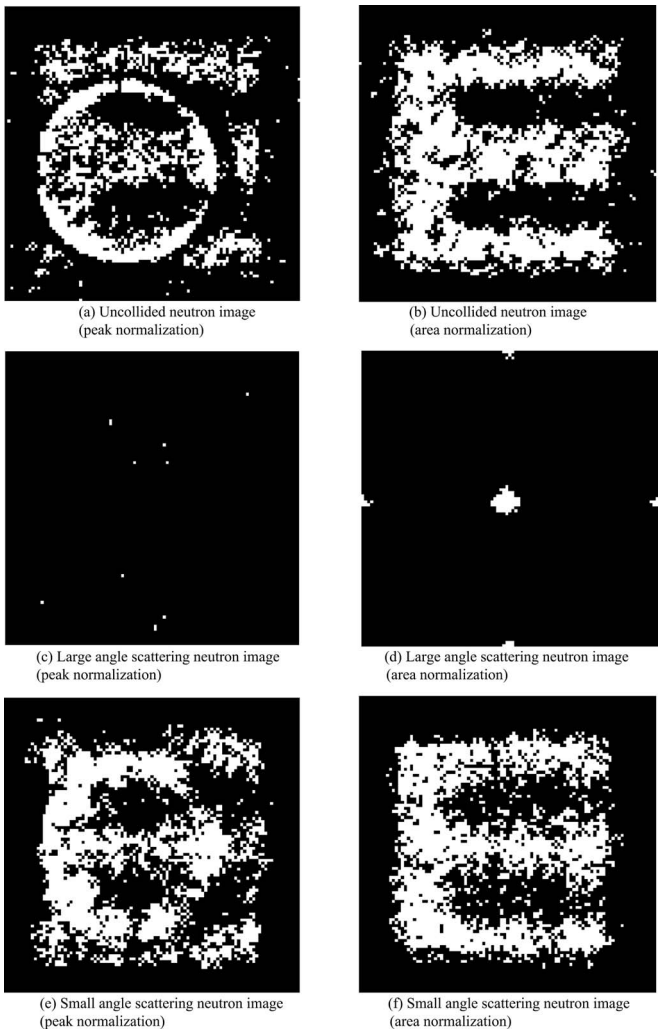

FIG. 15. The reconstruction of "E" character source during different encoding process: (a) uncollided neutron image (peak normalization), (b) uncollided neutron image (area normalization), (c) large angle scattering neutron image (peak normalization), (d) large angle scattering neutron image (area normalization), (e) small angle scattering neutron image (peak normalization), and (f) small angle scattering neutron image (area normalization).

(1) PSF simulation of a series of cylindrical apertures with different radius r_{ap}.
(2) Reconstruction by GA with peak normalization. Image reconstruction can be carried on using PSF obtained in (1).
(3) $q_r \sim r_{ap}$ curve obtainment.

The radius of the residual watermark r_3 is obtained by Hough transformation from reconstructed image in step (2). The residual watermark relative factor is defined as formula (5),

$$q_r = \frac{r_3}{r_{ap}}. \tag{5}$$

The $q_r \sim r_{ap}$ curve is plotted, and steps (1) and (2) are repeated at $q_r = 1$ to add data point on $q_r \sim r_{ap}$ curve.

The equivalent radius of the encoding aperture, i.e., r_{ap} corresponding to $q_r = 1$ is obtained by the $q_r \sim r_{ap}$ curve. In Figure 17, the equivalent radius can be obtained as 0.266 cm, which is close to 0.278 cm in Sec. V A.

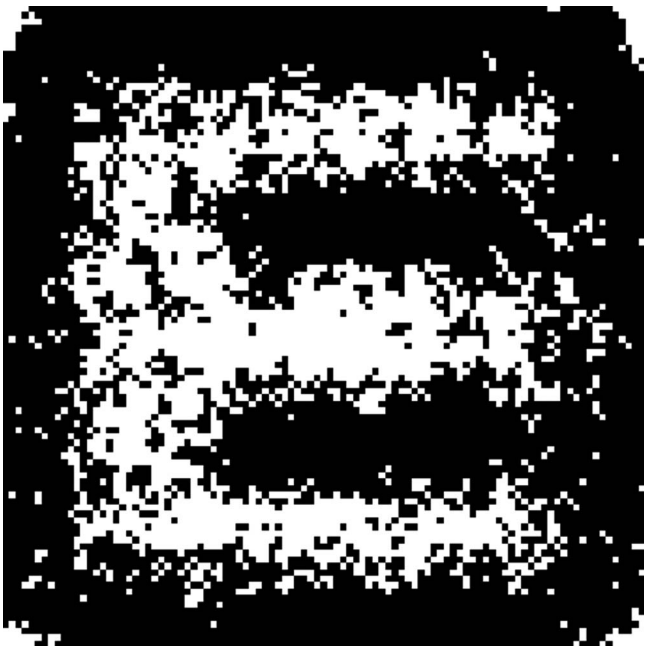

FIG. 16. The reconstruction result based on aperture defined by information of the residual watermark.

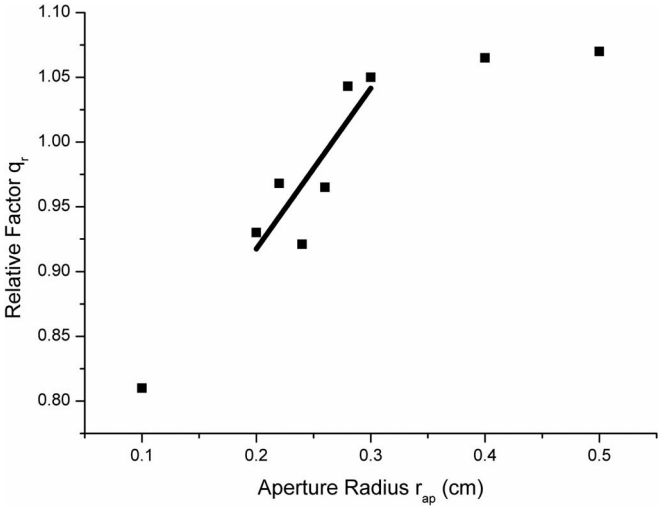

FIG. 17. The $q_r \sim r_{ap}$ curve.

Further, PSF was achieved by simulation with the cylindrical aperture in radius of 0.266 cm. And the source image was reconstructed by GA with area normalization (Figure 18). The correlation coefficient of this image is 0.7362, which is close to the reconstruction result shown in Figure 4(c).

VI. DISCUSSION

According to the results mentioned in Sec. IV, there is an important difference between area and peak normalization for image reconstruction. In area normalization, one constraint is added in the normalization process of changing raw simulation coded images into the data used in fitness calculation. Only the coded data, the parts of the source information on image plane, collected by the detectors are used for normalization. Whereas the peak normalization process by using maximum value in the source information on image plane is unbounded. The reconstruction based on peak normalization is affected more easily by the fluctuations than it based on area normalization. In this imaging system, the fluctuations are brought about mainly by the scattering neutrons of the aperture materials. Therefore, the residual watermark carrying some information of the encoding aperture could lucidly emerge in the reconstructed image.

FIG. 18. Reconstruction using the equivalent radius which equals to 0.266 cm.

As the radius is the selected parameter which characterizes the residual watermark in the case of the aperture with a round cross section channel, the parameters of straight lines, such as the length and orientation, are the suitable parameters which characterize the residual watermark in the case of the apertures with a square and a triangle cross section channel. And the straight line also can be detected by Hough transform. The residual watermark which appears under condition of the annular aperture[33] and pinhole array[34] would be discussed further.

Changing source size to get limit definitely corresponding to just presenting clear residual watermark in reconstructed results needs to be further studied.

The position of residual watermark overlying the reconstructed image is closely related to the search process of GA, the parameters of encoding aperture and the distribution of source.

The relationship between position of the residual watermark and the distribution of source should be studied necessarily, which may provide a criterion for establishing geometry central axis of imagining system combining with above relationship between the residual watermark and encoding aperture.

Compared with the result in Figure 7(c), the reconstructed image in Figure 8(c) gives obvious isolated points. The consistency between the source image and the reconstructed images is not well, and the feature of the reconstructed image cannot match with that of the implosion area. Both of the two reconstructed images are got by area normalization, but the neutron yield per pixel in Figure 7(c) is larger than that in Figure 8(c), in other words, the SNR per pixel in Figure 7(c) is larger than that in Figure 8(c). And then, the isolated points of reconstructed image in low SNR are more severe. The isolated points phenomenon should be studied, especially its influence on edge detection for the implosion images.

VII. CONCLUSION

The simulation system of neutron encoding image was established. The properties and the essential causes of residual watermark have been investigated. An identification algorithm of the equivalent radius of encoding aperture has been put forward based on residual watermark.

The distinguishing feature of reconstructed image embodies in the encoding image which comes from mixed information of source and encoding aperture. The information of equivalent radius aperture was obtained by employing GA based on peak normalization. Then, the reconstruction can be accomplished by employing GA based on area normalization

without knowing the PSF of actual aperture obtained by experiment or simulation.

Nevertheless the main information of the encoding aperture was determined, which can provide some applicable aspects, e.g., the identification of equivalent radius, and so on.

ACKNOWLEDGMENTS

This paper is supported by the NSAF Joint Fund set up by the National Natural Science Foundation of China and the Chinese Academy of Engineering Physics under Grant No. 10576022 and the Natural Science Foundation of China under Grant No. 10975113.

[1]K. A. Nugent and B. Luther-Davices, Opt. Commun. **49**, 393 (1984).
[2]D. Ress, R. A. Lerche, R. J. Ellis, S. M. Lane, and K. A. Nugent, Science **241**, 956 (1988).
[3]L. Disdier, A. Rouyer, D. C. Wilson, A. Fedotoff, C. Stoeckl, J.-L. Bourgade, V. Yu Glebov, J.-P. Garconnet, and W. Seka, Nucl. Instrum. Methods Phys. Res. A **489**, 496 (2002).
[4]L. Disdier, R. A. Lerche, J. L. Bourgade, and V. Yu. Glebov, Rev. Sci. Instrum. **75**, 2134 (2004).
[5]Y. W. Chen, K. Otsuki, and Z. Nakao, Rev. Sci. Instrum. **69**, 1966 (1998).
[6]K. A. Nugent, Rev. Sci. Instrum. **59**, 1658 (1988).
[7]A. Rouyer, Rev. Sci. Instrum. **74**, 1234 (2003).
[8]Z. Q. Zhao, J. B. Chen, and Y. K. Ding, Rev. Sci. Instrum. **77**, 073502 (2006).
[9]Y. L. Wu, H. S. Hu, and T. K. Zhang, Z. H. Li, Y. P. Zhan, Z. Y. Jiang, and J. Chu, Fusion Sci. Technol. **57**, 292 (2010).
[10]I. Thfoin, O. Landoas, T. Caillaud, L. Disdier, M. Vincent, J. L. Bourgade, B. Rosse, T. C. Sangster, V. Y. Glebov, G. Pien, and W. Armstrong, Rev. Sci. Instrum. **81**, 033503 (2010).
[11]D. Ress, IEEE Trans. Nucl. Sci. **37**, 155 (1990).
[12]Y. L. Wu, H. S. Hu, and T. K. Zhang, Z. H. Li and D. Chen, Rev. Sci. Instrum. **81**, 053502 (2010).
[13]M. Zbigniew, *Genetic Algorithms + Data Structures = Evolution Programs* (Springer, Berlin, 1999).
[14]A. Brindle, Ph.D. dissertation, University of Alberta, Edmonton, 1981.
[15]K. A. De Jong, Ph.D. dissertation, University of Michigan, Michigan, 1975.
[16]Y.-W. Chen, Z. Nakao, and K. Arakaki, Opt. Rev. **4**, 209 (1997).
[17]Y.-W. Chen, Z. Nakao, K. Arakaki, and S. Tamura, IEEE Trans. Nucl. Sci. **44**, 905 (1997).
[18]R. Singleton, IEEE Trans. Audio Electroacoust. **17**, 93 (1969).
[19]J. F. Briesmeister, MCNP-A general Monte Carlo *N*-particle transport code version 4C, LA-13709-M, Los Alamos Scientific Laboratory, 2000.
[20]D. C. Wilson, C. R. Christensen, G. L. Morgan, P. A. Bradley, and P. L. Gobby, Rev. Sci. Instrum. **74**, 1705 (2003).
[21]M. Zhou and S. D. Sun, *Genetic Algorithms: Theory and Applications* (National Defence Industry Press, Beijing, 1990), pp. 46–55 (in Chinese).
[22]G. L. Chen, X. F. Wang, Z. Q. Zhuang, and D. S. Wang, *Genetic Algorithm and its Applications* (People's Posts and Telecommunications, Beijing, 1996), pp. 334–340 (in Chinese).
[23]W. H. Richardson, J. Opt. Soc. Am. **62**, 55 (1972).
[24]L. B. Lucy, Astron. J. **79**, 745 (1974).
[25]Z. Zhao, Y. Ding, J. Dong, Y. Hao, S. Wu, L. Cao, and Y. Pu, Plasma Phys. Controlled Fusion **49**, 1145 (2007).
[26]D. Ress, R. A. Lerche, R. J. Ellis, S. M. Lane, and K. A. Nugent, Rev. Sci. Instrum. **59**, 1694 (1988).
[27]H. S. Hu, Q. S. Wang, J. Qin, Y. L. Wu, T. K. Zhang, Z. S. Xie, X. B. Jiang, G. G. Zhang, H. Xu, X. Y. Zheng, J. Zhang, W. H. Liu, Z. H. Li, B. P. Zhang, L. B. Li, Z. H. Song, X. P. Ouyang, J. Zhu, Y. L. Zhao, X. Q. Mi, Z. P. Dong, C. Li, Z. Y. Jiang, and Y. P. Zhan, IEEE Trans. Nucl. Sci. **55**, 2376 (2008).
[28]J. S. Lim, *Two-Dimensional Signal and Image Processing* (Prentice-Hall, Englewood Cliffs, 1990), pp. 536–540.
[29]G. L. Morgan *et al.*, Rev. Sci. Instrum. **72**(1), 865 (2001).
[30]D. H. Ballard, Pattern Recogn. **13**, 111 (1981).
[31]J. Illingworth and J. Kittler, Comput. Vis. Graph. Image Process. **44**, 87 (1988).
[32]See http://www.mathworks.com/matlabcentral/fileexchange/9898-hough-transform-for-circle-detection-gui for more information about websites.
[33]L. Disdier, A. Rouyer, I. Lantuejoul, O. Landoas, J. L. Bourgade, T. C. Sangster, V. Y. Glebov, and R. A. Lerche, Phys. Plasmas **13**, 056317 (2006).
[34]F. E. Merrill, D. Bower, R. Buckles, D. D. Clark, C. R. Danly *et al.*, Rev. Sci. Instrum. **83**, 10D317 (2012).